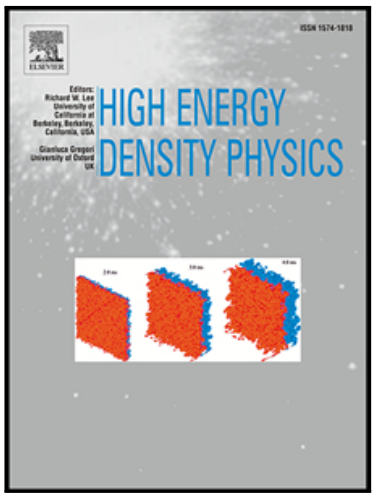

The effects of Magnetic Field Topology on Secondary Neutron Spectra in Magnetized Liner Inertial Fusion

B. Appelbe, J. Pecover, J. Chittenden

PII: S1574-1818(17)30005-8
DOI: 10.1016/j.hedp.2017.01.005
Reference: HEDP 585

To appear in: *High Energy Density Physics*

Received date: 23 November 2016
Revised date: 18 January 2017
Accepted date: 27 January 2017

Please cite this article as: B. Appelbe, J. Pecover, J. Chittenden, The effects of Magnetic Field Topology on Secondary Neutron Spectra in Magnetized Liner Inertial Fusion, *High Energy Density Physics* (2017), doi: 10.1016/j.hedp.2017.01.005

The effects of Magnetic Field Topology on Secondary Neutron Spectra in Magnetized Liner Inertial Fusion

B. Appelbe, J. Pecover and J. Chittenden

Centre for Inertial Fusion Studies, The Blackett Laboratory, Imperial College, London, SW7 2AZ, United Kingdom

Abstract

The Magnetized Liner Inertial Fusion (MagLIF) concept involves the compression of a magnetized fuel such that the stagnated fuel contains a magnetic field that can suppress heat flow losses and confine α particles. Magnetic confinement of α particles reduces the fuel ρR required for ignition. Recent work[1, 2] has demonstrated that the magnitude of the magnetic field in deuterium fuel can be inferred from the yields and spectra of secondary DT neutrons. In this work we investigate the potential for using the shape of the secondary neutron spectra to diagnose the magnetic field topology in the stagnated fuel. Three different field topologies that could possibly occur in MagLIF experiments are studied: (1) a cylindrical fuel column containing axial and azimuthal magnetic field components, (2) a fuel column which is pinched at the ends to form a magnetic mirror and (3) a fuel column that has a helical tube shape with magnetic field lines following the helical path of the tube's axis. Each topology is motivated by observations from experimental or simulated MagLIF data. For each topology we use a multi-physics model to investigate the shapes of the secondary neutron spectra emitted from a steady-state stagnated fuel column. It is found that the azimuthal and helical topologies are more suitable than the mirror topology for reproducing an asymmetry in the axial spectra that was observed in experiments. Gorgon MHD simulations of the MagLIF implosion in $1D$ are also carried out. These show that sufficient azimuthal magnetic field can penetrate from the liner into the fuel to qualitatively reproduce the observed spectral asymmetry.

Email address: bappelbe@ic.ac.uk ()

1. Introduction

The fuel ρR required to achieve ignition in Inertial Confinement Fusion (ICF) can be significantly reduced by the addition of a sufficiently large magnetic field.[3] The field reduces electron thermal conduction and confines the energetic α particles, thereby increasing the self-heating.[4] Magnetized Liner Inertial Fusion (MagLIF) is a fusion scheme currently being investigated at the Z facility, in which a magnetic field is compressed with the fuel in order to generate large magnetic fields at peak compression.[5, 6, 7]

MagLIF consists of a cylindrical, beryllium liner that is filled with fuel. A seed magnetic field of $\sim 10\,T$ parallel to the cylinder axis is entrained within the fuel. The liner is imploded onto the axis using a current of $\sim 20\,MA$, compressing the fuel and magnetic ($\mathbf{B}$) field to produce a hot, dense and magnetized plasma. The fuel ρR required for ignition in MagLIF is approximately 2 orders of magnitude less than in conventional ICF. Integrated experiments with a pure deuterium fuel have recently been carried out.[8] These experiments produced a yield of 2×10^{12} DD neutrons with a fuel temperature of $\sim 3\,keV$ and areal density $\sim 2\,mg\,cm^{-2}$ in a burn-time of a few nanoseconds.

A particularly novel diagnostic, which is the main focus of our work in this paper, was the use of secondary neutrons to measure fuel magnetization at stagnation.[1, 2] Nuclear reactions between deuteron particles (DD reactions) have two main branches

$$D + D \rightarrow \begin{cases} T\,(1.01\,MeV) + H^1\,(3.02\,MeV) & 50\,\%, \\ He^3\,(0.82\,MeV) + n\,(2.45\,MeV) & 50\,\%. \end{cases} \tag{1}$$

In a deuterium fuel the $2.45\,MeV$ neutrons produced from DD reactions are referred to as primary neutrons. The tritons produced in the other branch are fast particles that move through the deuterium fuel and can undergo a DT reaction to produce a neutron with a nominal energy of $14.1\,MeV$ according to

$$D + T \rightarrow He^4\,(3.5\,MeV) + n\,(14.1\,MeV)\,. \tag{2}$$

These neutrons are called secondary neutrons.[9] This is the only source of $14.1\,MeV$ neutrons in an initially pure deuterium fuel. The probability of a fast triton reacting depends primarily on the deuterium density and the path length of the triton in the fuel. The presence of a $\mathbf{B}$ field increases the path length.

Schmit, Knapp et al,[1, 2] developed a model in which the experimentally measured ratio of secondary to primary neutron yields, $\overline{Y}$, was used to infer the value of the parameter BR (axial magnetic field strength times fuel radius). This model used a cylindrical fuel configuration with an axial **B** field. A value of $BR \approx 0.34\,T\,m$ was inferred from the experiments. This value suggests that the fuel radius is greater than the Larmor radius of a $1.01\,MeV$ triton particle meaning that tritons can indeed be magnetically confined in MagLIF. For example, for a fuel radius of $100\,\mu m$ the magnitude of the **B** field is $3.4 \times 10^3\,T$. In this field the Larmor radius of a $1.01\,MeV$ triton is $74\,\mu m$. This suggests that α particles will also be confined (a $3.45\,MeV$ α particles has a Larmor radius of $91\,\mu m$).

The model also reproduced many features of the secondary neutron spectra emitted in the axial and radial directions. The radial spectrum shows a single peak near $14.1\,MeV$ whilst the axial spectrum displays two peaks at higher and lower energies. The axial spectrum is noticeably broader than the radial spectrum. These features are illustrated schematically in fig. 1. However, one feature of the measured spectra that has not yet been explained is the asymmetry of the double-peaked axial spectrum, also illustrated in fig. 1. In the reported experimental data[1] the intensity of the peak at higher energy was approximately 50% greater than the intensity of the peak at lower energy. In this work we show that a **B** field which is not purely axial could cause a net drift of tritons resulting in such an asymmetry.

We identify three **B** field configurations that could cause this effect, each motivated by observations of experimental or simulation data. A schematic illustration of the different topologies is shown in fig. 2. The first is an axial **B** field with an additional azimuthal field component within the fuel, such as that generated by a current flowing in the axial direction. We refer to this as the "azimuthal topology". The second is an axial **B** field that is pinched at the two ends of the cylinder, forming a **B** field structure similar to that of a magnetic mirror. This is referred to as the "mirror topology". The final configuration is where the **B** field lines follow a helical trajectory in a fuel column that takes the form of a helical tube. We refer to this as the "helical topology". We develop a parameterized model that allows us to investigate each configuration.

The contents of the paper are as follows. In section 2 we discuss the intuitive ideas behind the work and describe the model used to investigate the secondary neutron spectra. A detailed analysis of the azimuthal, mirror and helical topology and resulting spectra is contained in sections 3, 4 and

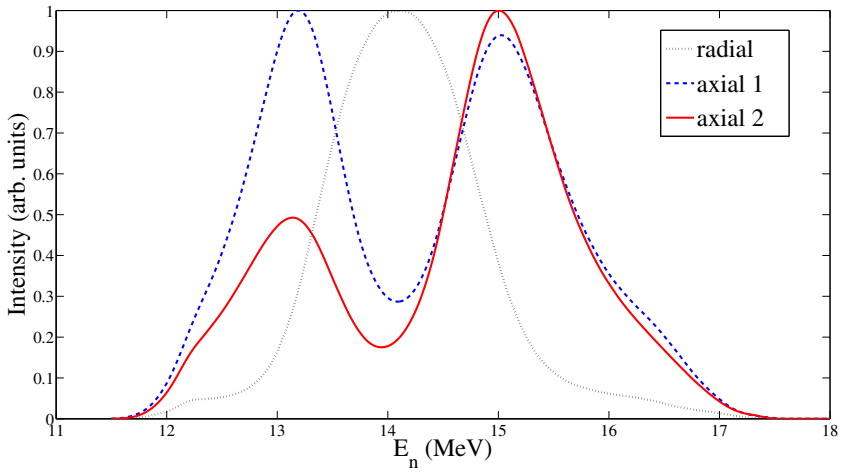

Figure 1: Schematic illustration of secondary neutron spectra produced in MagLIF in the radial and axial directions. "axial 1" is an axially emitted spectrum for a **B** field directed along the cylinder axis. "axial 2" is an axially emitted spectrum in which there is an additional azimuthal **B** field near the edge of the cylinder. The "radial" curve is the radially emitted spectrum for a **B** field directed along the cylinder axis only. Parameter values used to calculate these spectra are listed in table 1.

5, respectively. Section 6 discusses results from a series of $1D$ Gorgon MHD simulations in which the azimuthal topology is present. Finally, a summary and some conclusions are contained in section 7.

2. Background Ideas and Description of Model

The tritons produced in thermonuclear DD reactions are emitted approximately isotropically. [1] The main spectra features illustrated in fig. 1 can be explained by assuming that tritons are emitted isotropically on the axis of a cylinder of deuterium plasma with high aspect ratio ($h \gg r$). If the cylinder is unmagnetized then tritons emitted radially will have a much shorter path

[1] Deviations from isotropy can be caused by bulk fluid motion of the reacting plasma. This deviation scales with $\mathcal{O}\left(\frac{v_f}{v_t}\right)$ for $v_f \ll v_t$ where v_t is triton velocity and v_f is bulk fluid velocity. A $1.01\,MeV$ triton has a velocity of $v_t = 8 \times 10^6\, ms^{-1}$. The implosion velocity in MagLIF is approximately $7 \times 10^4\, ms^{-1}$ and if we take this as an estimate value for v_f then we can see that deviations from isotropic emission are small.

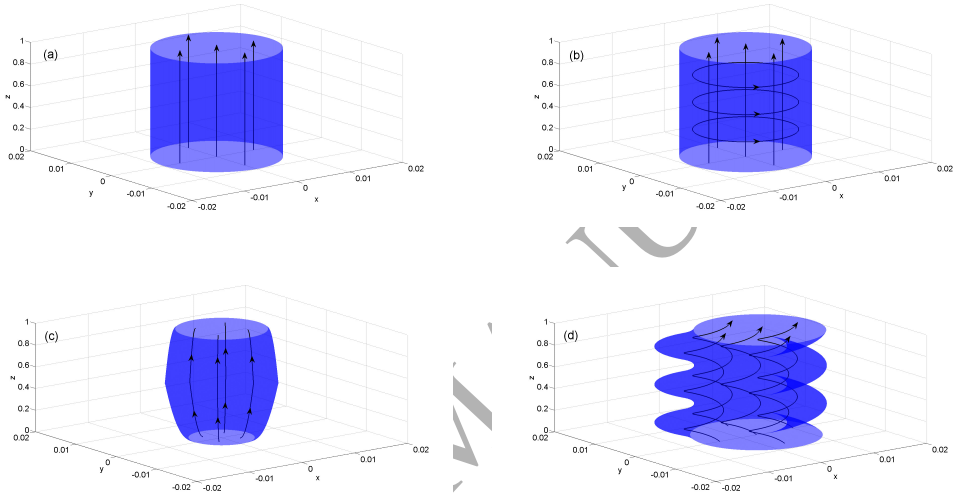

Figure 2: Schematic illustration of the different field topologies under consideration. The blue surface indicates the boundary of the fuel column while the black lines indicate magnetic field components. Normalized units are used for the axes. (a) A cylindrical fuel column with axial magnetic field lines. This set-up results in axially-emitted secondary neutron spectrum that is symmetric with two peaks of very similar intensity. (b) The azimuthal topology. This is similar to (a) but with an additional azimuthal field component. (c) The mirror topology. The lower end of the fuel column is pinched to a smaller radius than the upper end to generate a net upward drift of tritons. (d) The helical topology. The centre of the fuel column follows a helical trajectory and has a constant radius. Field lines are parallel to this helix.

length in the plasma before they escape than those emitted axially. Since the probability of a triton reacting increases proportionally to its path length in the plasma this means that the majority of neutrons detected by a radially located detector will be due to reactions of tritons moving axially which emit neutrons orthogonal to the triton motion. Therefore, the energy spectrum of neutrons emitted in the radial direction will be relatively narrow because of the small centre-of-mass velocity component along the detector line-of-sight. In contrast, the energy spectrum of neutrons emitted in the axial direction is dominated by tritons that are moving towards and away from the detector. Therefore, the detected neutrons will have an energy upshift (for tritons moving towards the detector) and downshift (away from the detector) resulting in the double-peaked structure of the "axial 1" spectrum in fig. 1.

If we introduce an axial **B** field then only the radial component of a triton's velocity will be affected. As the strength of the axial field is increased then the effective path length of radially emitted tritons is increased as they become more magnetized. This means that the contribution to the axial neutron spectrum from tritons that do not have an axial velocity component becomes larger. Since these neutrons are emitted orthogonally to the tritons' velocity the result is that as the axial field strength is increased a greater proportion of axially emitted neutrons will have an energy close to $14.1\,MeV$. This causes the trough between the two peaks of the axial spectrum to become shallower as the axial field strength increases. However, the two peaks continue to have an intensity that is almost equal and so this picture is not sufficient to explain the asymmetry in the spectrum labelled "axial 2" in fig. 1. In order to produce this spectrum we need more neutrons to be produced by tritons moving towards the detector than away from it. If we assume that the tritons are produced uniformly along the cylinder axis and that the deuterium plasma is homogeneous then this means that there must be some mechanism by which the initially isotropic tritons move preferentially in one axial direction. A **B** field that either has non-axial components or varies in strength along the axis could provide such a mechanism. The azimuthal, mirror and helical topologies are all suitable candidates.

For each topology we introduce three parameters to quantify the strength and direction of the **B** field throughout the fuel column. In each case one of these parameters (denoted by $\langle BR \rangle$) is a measure of the field strength. Previous work in which only a uniform axial field was considered[3] has identified BR (where B is the magnetic field strength and R is fuel radius) as a key parameter for studying fast ion transport in magnetized cylin-

ders. It has been shown that MagLIF experiments correspond to a value of $BR = 0.3 - 0.4\,T\,m$.[1, 2] We choose similar values for our $\langle BR \rangle$ parameter, which is a generalization of the BR parameter that allows for non-axial fields. The remaining two parameters are used to define the shape of the field lines for each topology. For the azimuthal topology these parameters define the relative strengths of the axial and azimuthal field components and how far the azimuthal field penetrates into the fuel (ζ, γ). For the mirror topology the two parameters describe how pinched the bottom and top ends of the fuel column are relative to the middle (λ_1, λ_2). For the helical topology the parameters define the radius and pitch of a helical path which the field lines follow (H_r, H_p).

When the **B** field is specified we can then study how tritons drift along the axis of the fuel column, resulting in asymmetric axial neutron spectra. We have developed a multi-physics model to simulate triton dynamics and production of secondary spectra. The model uses a steady-state radial profile for deuterium density and temperature of the form

$$T_i(r) = T_{i0} - (T_{i0} - T_{iR})\,(r/R)^{\nu}, \tag{3}$$

$$\rho(r) = \rho_0 T_{i0}/T_i(r), \tag{4}$$

where we have assumed that the fuel is isobaric, $\nu \approx 1.5 - 3$ and R represents the radius of the fuel column. The radial variable r is measured from the cylinder axis (or from the helix axis for the helical topology). T_{i0} and ρ_0 represent the on-axis ion temperature and density, respectively, while T_{iR} represents the temperature at the edge of the fuel.

We choose values for ρ_0 in the range $100 - 200\,kg\,m^{-3}$ which, for a cylinder radius $R = 100\,\mu m$, gives an areal density range of $2.8 - 5.6 \times 10^{-2}\,kg\,m^{-2}$. We use a cylinder height of $h = 1\,cm$. Unless otherwise stated, we use values of $\nu = 1.8$, $T_{i0} = 5\,keV$ and $T_{iR} = 0.1\,keV$. This low value of T_{iR} means that that very few tritons are produced in the outer region of the fuel column. However, this region forms a cold, dense deuterium plasma in which the tritons can react if they are transported radially outwards. X-ray emission images from experiments show a hot fuel plasma column with radius $30 - 70\,\mu m$ and height $6\,mm$ while spectroscopy data suggests a burn-averaged deuterium fuel ρR of $2 \times 10^{-2}\,kg\,m^{-2}$.[8] The plasma column that we use in our simulations, which contains both hot and cold plasma, has a similar aspect ratio to the X-ray images and a slightly larger areal density that is primarily due to the cold, dense layer at the edge of the cylinder.

The neutron energy spectrum from DD reactions can be calculated as a function of deuterium density and temperature.[10, 11, 12] The burn-averaged ion temperature can be obtained from the width of this spectrum. For the values of ν, T_{i0} and T_{iR} given above we get a burn-averaged ion temperature of $3.2\,keV$. Tritons produced from DD reactions will also be thermally broadened about the $1.01\,MeV$ nominal energy.[13] Computational triton particles are created at 400 locations uniformly spaced throughout the pinch. Each computational particle has a weighting specified by the production rate at that location and an energy randomly selected from a gaussian distribution of the same width as the thermally broadened triton spectrum. At each location, 2.5×10^3 computational particles are created with their initial velocity vector uniformly distributed over 4π.

The trajectories of the computational particles are evolved using the Boris algorithm[14] for the specified **B** field topology until they escape from the fuel or a time period of $2\,ns$ has elapsed. The triton motion cannot be calculated using the guiding centre approximation since the plasma conditions vary significantly over a length scale similar to the triton's Larmor radius. Coulomb collisions between the tritons and the background plasma are modelled using a Fokker-Planck model that calculates both slowing and diffusion of the particles.[15, 16] Reactions between a triton particle and the background deuterium plasma are also calculated at every time step. Given the deuterium density, temperature and the triton particle weighting, the secondary DT yield can be calculated. In order to generate a secondary neutron spectrum we specify a number of detector locations. We then use a semi-analytic solution to produce the thermally broadened secondary neutron spectrum emitted towards each detector.[17, 18] Prior to simulations the spectra produced by this solution are tabulated for a large number of particle energies, background plasma temperatures and emission angles, allowing the required spectrum to be obtained quickly at each time-step. The summation of spectra produced by each particle at each time-step then gives the secondary neutron spectrum emitted in each specified direction. All reaction cross-sections used are taken from the ENDF database.[19]

This model allows us to simulate secondary neutron spectra for a wide variety of stagnation conditions. However, the large number of input parameters (densities, temperatures, **B** field topologies, etc.) make it difficult to represent the results from an exhaustive parameter scan. Therefore, our approach is to identify the set of parameter values that best represent the asymmetry of the axial neutron spectrum illustrated in fig. 1 for each **B**

field topology and to investigate how sensitive the spectra are to changes in parameter values.

3. The azimuthal topology

Experiments at the Z facility compress the seed axial $\mathbf{B}$ field to a peak value of $\sim 10^3\,T$. This compression is achieved using an azimuthal $\mathbf{B}$ field that also reaches $\sim 10^4\,T$ at peak current.[7] The current flows in the beryllium liner and so, ideally, the azimuthal field is zero inside the fuel. However, MHD simulations show that current and, consequently, azimuthal field can penetrate into the fuel region.[20]

The presence of an azimuthal $\mathbf{B}$ field in the fuel can result in tritons flowing preferentially in one axial direction due to the phenomenon of singular orbits.[21, 22] These are illustrated in 2 dimensions in fig. 3 for the situation in which no axial $\mathbf{B}$ field is present. As the particle moves back and forth across the axis, the direction of the $\mathbf{B}$ field that it sees switches direction. This causes the direction of gyro-motion to reverse and so particles can move along the axis rather than being trapped in a conventional Larmor orbit. Figure 3 illustrates singular orbits drifting both parallel and anti-parallel to the current flow. However, it is found that singular orbits in the parallel direction dominate for two reasons: a greater range of initial pitch angles, θ_0, result in singular orbits in the parallel rather than anti-parallel direction and also singular orbits in the parallel direction can have a larger axial drift velocity.

When we include an axial $\mathbf{B}$ field the singular orbit behaviour becomes inherently 3 dimensional but the drift remains greater in the parallel direction, both in terms of the number of particles and the drift velocities.

3.1. Field parameterization for the azimuthal topology

We introduce three parameters to describe the azimuthal field topology. Analogous to the BR parameter for cylinders with a purely axial field,[3] we define a parameter $\langle BR\rangle$ as a measure of integrated field strength

$$\langle BR\rangle = \int_0^R \sqrt{B_z^2 + B_\theta^2}\,dr, \tag{5}$$

where R is the cylinder radius and B_z and B_θ are the magnitudes of the axial and azimuthal field components, respectively. We let B_z be constant while

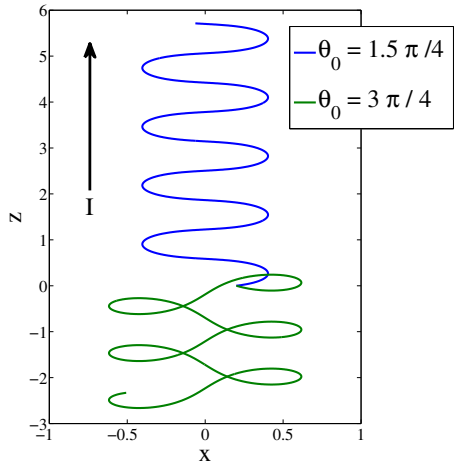

Figure 3: An illustration of the singular orbit phenomenon for a positively charged particle in an azimuthal **B** field generated by a current of uniform density flowing in the $+z$ direction. The blue (green) curve represents a singular orbit parallel (anti-parallel) to the current flow. As shown here, singular orbits parallel to current flow experience a greater axial displacement since they undergo less rotation in the **B** field. The variable θ_0 is the initial pitch angle of a particle's trajectory with respect to the $+z$ axis. Normalized units are chosen such that the Larmor radius at $x = 1$ is 0.1. The strength of the **B** field is 0 at $x = 0$ and rises linearly as $|x|$ increases. The **B** field is directed into the page for $x > 0$ and outwards for $x < 0$.

B_θ varies with radius according to

$$B_\theta(r) = \left(\frac{r}{R}\right)^\gamma B_\theta^R, \tag{6}$$

where B_θ^R denotes the magnitude of the azimuthal field at the cylinder edge and γ represents the current distribution in the cylinder. For $\gamma = 1$, current is uniformly distributed while large values of γ correspond to a skin current flowing near the cylinder edge.

We choose three independent parameters γ, $\langle BR \rangle$ and ζ, where ζ is the ratio of the azimuthal field strength at the cylinder edge to the axial field strength

$$\zeta = \frac{B_\theta^R}{B_z}. \tag{7}$$

We can then obtain B_z from the parameters as follows

$$B_z = \frac{\langle BR \rangle}{R \int_0^1 \sqrt{1 + x^\gamma \zeta} dx}. \tag{8}$$

We assume that the current is flowing in the $+z$ direction such that the B_θ field is directed anti-clockwise when viewed from the $+z$ direction.

3.2. Secondary spectra for the azimuthal topology

The model described in section 2 can be used to produce secondary neutron spectra from the azimuthal topology when values are specified for the parameter set $(\langle BR \rangle, \gamma, \zeta)$. These values are chosen with the goal of creating an asymmetry between the two peaks in the axial spectra. Results from a selection of simulations are shown in figs. 4 and 5. The spectra produced from each simulation are numbered and the corresponding parameter values are listed in table 1.

The spectra labelled 1 in fig. 4 are produced with parameter values of $\langle BR \rangle = 0.4\,T\,m$ and $\zeta = 0$. This corresponds to a cylinder with no azimuthal field and a uniform axial field of $4 \times 10^3\,T$. The spectra emitted in the $+z$ and $-z$ directions are identical, as we expect since the axial field does not cause a net axial drift of tritons. These spectra are approximately symmetric, with two peaks that have similar intensities. The slightly lower intensity of the higher energy peak is caused by the kinematics of the DT reaction. For triton beam particles with $E_t \leq 1.01\,MeV$ neutrons produced in the forward (backward) direction have an energy in the range

$[14.1, 17.2]\ MeV$ ($[11.8, 14.1]\ MeV$). Therefore, even though the differential cross-section favours neutron production in the forward direction, the greater energy spread of the higher energy neutrons causes the intensity of the higher energy peak to be slightly less than that of the lower energy peak.

The spectra labelled 2 in fig. 4 are produced with parameter values $\langle BR \rangle = 0.4\,T\,m$, $\gamma = 10$ and $\zeta = 1$. This corresponds to a uniform B_z field of $3.8 \times 10^3\,T$ and a B_θ field with a value of $3.8 \times 10^3\,T$ at the cylinder edge and a value of $66\,T$ at $0.66R$. The introduction of this B_θ field has a negligible effect on the spectrum emitted in the radial direction but there is a significant change in the axial spectra. These become highly asymmetric with the higher energy peak in the $+z$ direction having an intensity more than 1.5 times that of the lower energy peak. The reverse is the case for the $-z$ direction and this result is consistent with the net axial drift of tritons in the $+z$ direction. The remaining spectra in fig. 4 show the effect of varying the $\langle BR \rangle$ parameter. The asymmetry in the axial spectra is greater for smaller values of $\langle BR \rangle$. This is because the B_z is not strong enough to locally confine the tritons and they can move to regions of higher B_θ where singular orbit motions cause them to move in the $+z$ direction. As $\langle BR \rangle$ is increased, the tritons become more locally confined and so a smaller fraction of the particles can undergo axial drift.

Figure 5 illustrates some results in which $\langle BR \rangle$ is kept constant while γ and ζ are varied. As we would expect, smaller values of γ (e.g. spectra no. 6) result in more asymmetric axial spectra as the azimuthal field penetrates further into the cylinder. However, the asymmetry remains apparent even as γ is increased above $\gamma = 10$. The spectra labelled 7 in fig. 5 correspond to $\gamma = 20$. At this value, B_θ has a value of $3.8 \times 10^3\,T$ at the cylinder edge but drops off very rapidly such that $B_\theta < 100\,T$ for $r < 0.83R$. Therefore, if the azimuthal $\mathbf{B}$ field is sufficiently large at the edge of the cylinder then it does not need to penetrate far into the fuel in order to affect the shape of the axial spectra.

The spectra labelled 8 and 9 in fig. 5 show the effect of varying ζ. This parameter can be varied over a large range whilst still producing asymmetry in the axial spectra including cases where B_θ at the cylinder edge is significantly smaller than B_z (as in spectra no. 8). As $\zeta \to 0$ the case of a purely B_z field is recovered.

Table 1 lists results for yield ratio ($\overline{Y}$) and the spectra FWHM in the radial (denoted by Δ_R) and $+z$ (Δ_{+z}) directions. Values of $\Delta_{+z} < 2\,MeV$ occur when the intensity of the lower energy peak is less than half that of

Table 1: This table lists data relating to the spectra plotted in figs. 4 and 5. The azimuthal field topology parameters ($\langle BR \rangle$, γ, ζ) used to generate each set of spectra are given together with the FWHM values of the spectra (Δ_R for the radial spectrum and Δ_{+z} for the axial spectrum). The ratio of secondary to primary neutron yields ($\overline{Y}$) for each simulation is also listed. Values of $\rho_0 = 200\,kg\,m^{-3}$, $T_{i0} = 5\,keV$, $T_{iR} = 0.1\,keV$, $\nu = 1.8$, $h = 1\,cm$, $R = 100\,\mu m$ were used for all these simulations. The spectrum labelled "axial 2" in fig. 1 is produced using the same parameters as spectra no. 3 while the parameters for the spectra labelled "radial" and "axial 1" are listed in the final row of the table.

Spec no.	$\langle BR \rangle$ $(T\,m)$	γ	ζ	$\overline{Y}$	Δ_R (MeV)	Δ_{+z} (MeV)
1	0.4	–	0.0	2.10×10^{-2}	1.87	2.80
2	0.4	10	1.0	1.93×10^{-2}	1.85	2.64
3	0.3	10	1.0	9.80×10^{-3}	1.53	1.19
4	0.5	10	1.0	2.95×10^{-2}	2.04	2.53
5	0.6	10	1.0	3.79×10^{-2}	2.13	2.45
6	0.4	5	1.0	1.80×10^{-2}	1.85	1.34
7	0.4	20	1.0	2.01×10^{-2}	1.85	2.78
8	0.4	10	0.5	2.01×10^{-2}	1.85	2.74
9	0.4	10	2.0	1.83×10^{-2}	1.84	1.35
axial 1	0.3	–	0.0	1.05×10^{-2}	1.53	3.11

the higher energy peak. Integrated MagLIF experiments measured values of $\overline{Y} = 2.8 \times 10^{-2}$, $\Delta_R = 2.3\,MeV$ and $\Delta_{+z} = 3.25\,MeV$, respectively.[1] The values of $\overline{Y}$ and Δ_R are very similar for all simulations with $\langle BR \rangle = 0.4\,T\,m$. This is because the level of magnetic confinement is primarily determined by $\langle BR \rangle$ and so variations in γ and ζ have little effect on the ability of tritons to radially escape for a fixed $\langle BR \rangle$ value.

Finally, we note that the axial spectrum with a more intense peak at the higher energy side is produced in the same direction as current flow. This is consistent with the experimental data from integrated MagLIF experiments in which a nTOF detector was located axially in the direction of current flow.

From the results just described we can conclude that there is a broad range of parameter space for the azimuthal topology in which asymmetry of the axial spectra can be produced.

4. The mirror topology

The next topology that we investigate is that of an asymmetric magnetic mirror. MHD simulations of MagLIF in 2D have shown that the ends of the

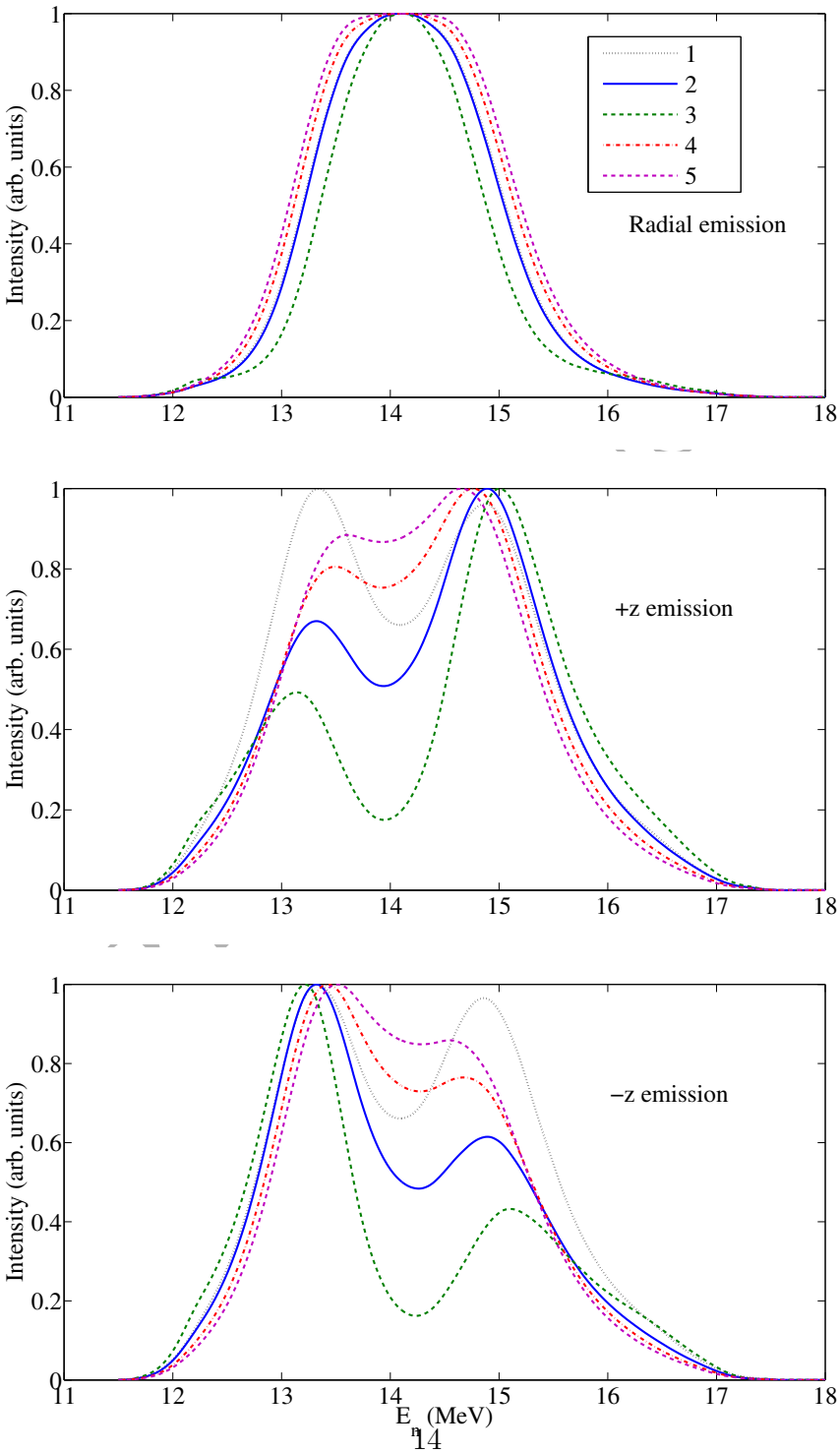

Figure 4: Secondary spectra results for simulations of the azimuthal topology. Spectra emitted in the radial, $+z$ and $-z$ directions are shown in the top, middle and bottom diagrams, respectively. The parameters used to produce each set of spectra are listed in table 1. The key shown in the top diagram also applies to the middle and bottom diagrams. Spectra no. 1 are for a purely axial field with $\langle BR \rangle = 0.4\,T\,m$. In this case, the axially emitted spectra are close to symmetric. Spectra no. 2 have the same $\langle BR \rangle$ value but with a non-zero azimuthal field component ($\gamma = 10$, $\zeta = 1.0$) causing the axially

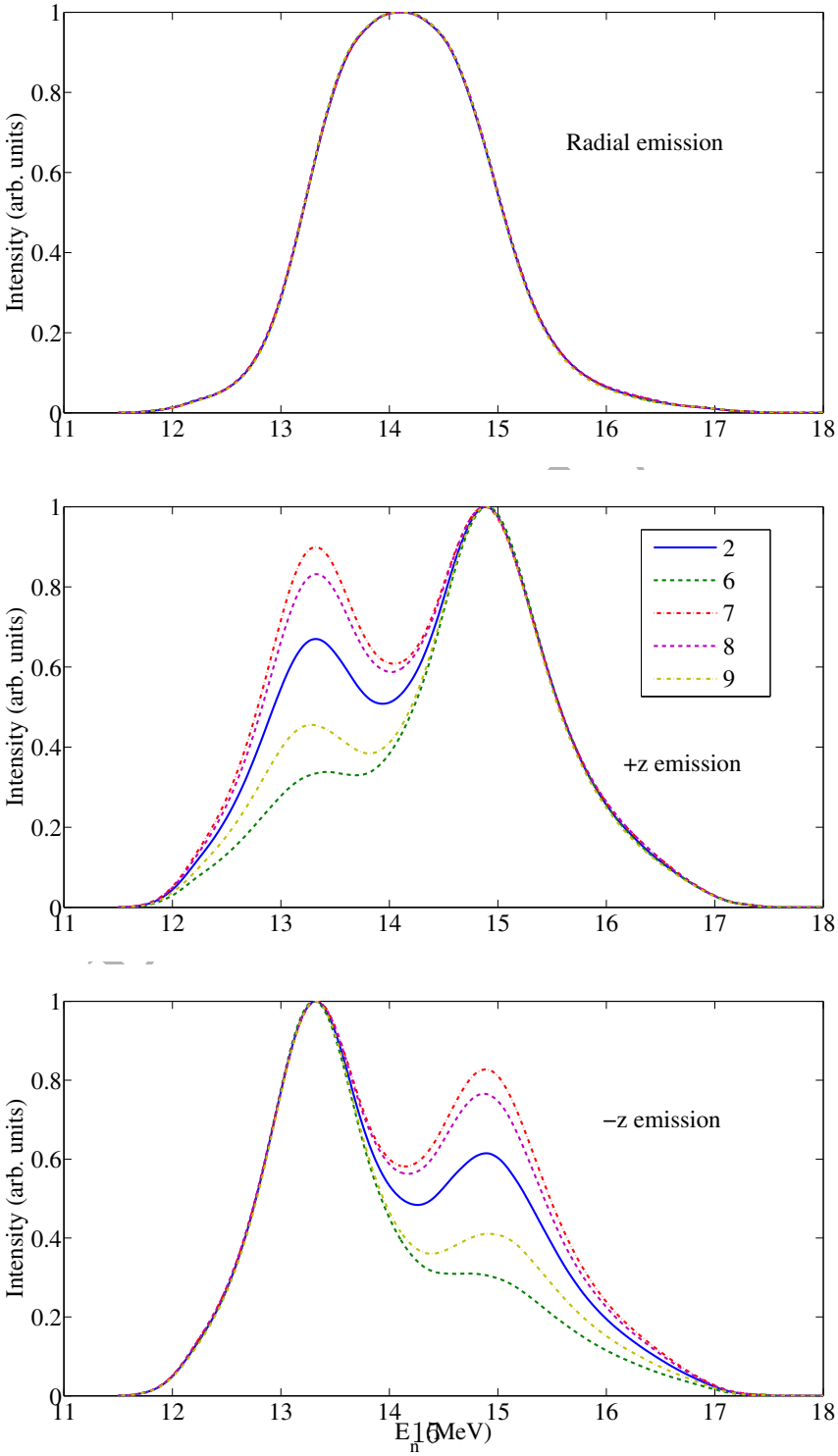

Figure 5: Secondary spectra for sets of parameter values given in table 1. All spectra in this figure correspond to $\langle BR \rangle = 0.4\,T\,m$. A comparison of spectra nos. 7, 2 and 6 illustrates the effect of the azimuthal field penetrating further into the fuel (γ = 20, 10 and 5, respectively). A greater penetration depth (i.e. reduced γ value) increases the asymmetry of the axial spectra. A comparison of spectra nos. 8, 2 and 9 illustrates the effect of varying the ratio of azimuthal to axial field strength (ζ = 0.5, 1.0 and 2.0,

liner in contact with the electrodes can compress more than the centre.[23] This results in a larger B_z field at the ends than in the centre of the cylinder and so the **B** field in the stagnated deuterium plasma resembles a magnetic mirror. If tritons are emitted at the centre of this cylinder then their axial velocity component will be reduced as they move towards the ends of the cylinder. If we now assume that the magnetic mirror configuration is asymmetric such that the bottom of the cylinder is more compressed than the top then the axial velocity component of those tritons moving downwards will decrease faster than that of tritons moving upwards. Such a configuration will result in a net axial drift of tritons in the upward direction.

4.1. Field parameterization for the mirror topology

In order to parameterize the fields in a magnetic mirror we assume that the cylinder centre is located at $z = 0$ with ends at $z = \pm\frac{h}{2}$. We use the parameters $\langle BR\rangle$, λ_1 and λ_2 to define the fields. In this case $\langle BR\rangle$ is the axial field strength (assumed independent of r) times cylinder radius at $z = 0$ (denoted by R_0). The cylinder radius at $z = \pm\frac{h}{2}$ is then given by

$$R_{-h/2} = \lambda_1 R_0, \tag{9}$$

$$R_{+h/2} = \lambda_2\lambda_1 R_0. \tag{10}$$

The cylinder radius, $R(z)$, varies according to a power law between the middle and ends of the fuel column as follows

$$R(z) = \begin{cases} R_{+h/2} + \left(R_0 - R_{+h/2}\right)\left(\frac{h}{2} - z\right)^{0.2} & if \quad z \geq 0, \\ R_{-h/2} + \left(R_0 - R_{-h/2}\right)\left(\frac{h}{2} + z\right)^{0.2} & if \quad z < 0. \end{cases} \tag{11}$$

The exponent value of 0.2 was chosen such that the fuel column radius changes slowly near the centre but pinches rapidly near the ends to the radii $R_{\pm h/2}$. With this geometry, and assuming that total magnetic flux in the vertical direction is conserved, we can use $\nabla.\mathbf{B} = 0$ to calculate the magnetic fields as a function of position (r, z) in the cylinder. This results in

$$B_z = \left(\frac{R_0}{R(z)}\right)^2 B_{z_0}, \tag{12}$$

$$B_r = \begin{cases} -\frac{r}{h}\frac{2B_{z_0}R_0^3}{R(z)^3}\left(1 - \lambda_2\lambda_1\right) & if \quad z \geq 0, \\ -\frac{r}{h}\frac{2B_{z_0}R_0^3}{R(z)^3}\left(\lambda_1 - 1\right) & if \quad z < 0. \end{cases} \tag{13}$$

Here, the B_r component arises from the fact that the field lines become more bunched as the radius decreases while conservation of total axial magnetic flux results in B_z increasing as radius decreases.

4.2. Secondary spectra for the mirror topology

Simulation results for the mirror topology are shown in fig. 6 with the corresponding parameter values given in table 2. The spectra labelled 1 in fig. 6 are the best representation that we find of the asymmetric feature in the axial spectra. For the spectrum emitted in the $+z$ direction, the lower energy peak has an intensity of approximately 0.75 times that of the higher energy peak. This result is obtained for parameter values of $\lambda_1 = 0.8$ and $\lambda_2 = 1.25$. This means that the fuel has radii of $80\,\mu m$ at the bottom and $100\,\mu m$ at the middle and top. Therefore, the fuel column is pinched at the bottom end but is cylindrical with no pinching for $z > 0$. Reducing the value of λ_2 causes the top end of the fuel column to pinch. This causes the asymmetry in the axial spectra to be reduced since triton motion in the axial up direction is being restricted. This is illustrated by the spectra labelled 2 in fig. 6 in which a value of $\lambda_2 = 1.1$ (giving a radius of $88\,\mu m$ at the top) is used.

Reducing λ_1 causes the bottom end of the fuel column to become more pinched. However, as illustrated by spectra 3 in fig. 6 ($\lambda_1 = 0.7$), this does not result in a more asymmetric spectrum. This is because as a triton moves towards the regions of more compressed B_z field, the particle's axial velocity is reduced and reverses direction. As this occurs, energy conservation causes the radial component of the particle's velocity to increase. When λ_1 is reduced from 0.8 to 0.7 the increased population of radially moving tritons causes the radially emitted neutron spectrum to broaden and the axial spectra to become less asymmetric. As can be seen in fig. 6, a reduction in the asymmetry of axial spectra is accompanied by an increase in the width of the radial spectra Δ_R due to this effect. Therefore, in general as we try to increase the magnetic mirror effect (say by reducing λ_1) to induce an axial drift of tritons, there is an unavoidable increase in the radial momentum of tritons which contributes significantly to the shape of the spectra.

Finally, we note that in defining the mirror topology we used an exponent value of 0.2 in (11). This value was chosen such that the fuel column is nearly cylindrical for much of its length but narrows rapidly near the ends. This means that changes in the triton axial velocity occur mostly near the ends. Effectively, the tritons "bounce" when they reach the end regions. For larger

Table 2: This table lists data relating to the spectra plotted in fig. 6. The mirror field topology parameters ($\langle BR\rangle$, λ_1, λ_2) used to generate each set of spectra are given together with the FWHM values of the spectra (Δ_R for the radial spectrum and Δ_{+z} for the axial spectrum). The ratio of secondary to primary neutron yields ($\overline{Y}$) for each simulation is also listed. The same values of T_{i0}, T_{iR}, ν, h and R are used as in table 1. A value of $\rho_0 = 100\,kg\,m^{-3}$ was used for the mirror simulations.

Spec no.	$\langle BR\rangle$ $(T\,m)$	λ_1	λ_2	$\overline{Y}$	Δ_R (MeV)	Δ_{+z} (MeV)
1	0.3	0.8	1.25	8.25×10^{-3}	1.96	2.95
2	0.3	0.8	1.1	9.42×10^{-3}	2.06	3.02
3	0.3	0.7	1.25	1.03×10^{-2}	2.17	2.84
4	0.4	0.8	1.25	1.66×10^{-2}	2.31	2.47
5	0.4	0.9	1.1	1.58×10^{-2}	2.24	2.60

exponent values the asymmetry in the axial spectra is negligible because the time in which a triton can have an increased radial momentum is increased.

We can summarise our results for the mirror topology by stating that asymmetry of the axial spectra can be obtained in this topology. However, in order to achieve significant asymmetry, we require a fuel column which is pinched at one end but has a radius similar to the middle of the fuel column at the other end. There is currently no experimental or theoretical evidence for this in MagLIF.

5. The helical topology

The final topology that we investigate is motivated by experimental MagLIF data. X-ray emission images from the hot plasma at stagnation apparently show a helical structure.[8, 24] This is consistent with the observation of a helix-like instability growth in liner-only experiments.[25] These results suggest that the stagnated fuel may take the form of a helical tube rather than a cylindrical column. If we assume that the initially axial field gets compressed into this helical tube shape then the field lines will be curved in a manner that can cause a drift of tritons. In this section we investigate the potential for such a field topology to cause a net axial drift of tritons.

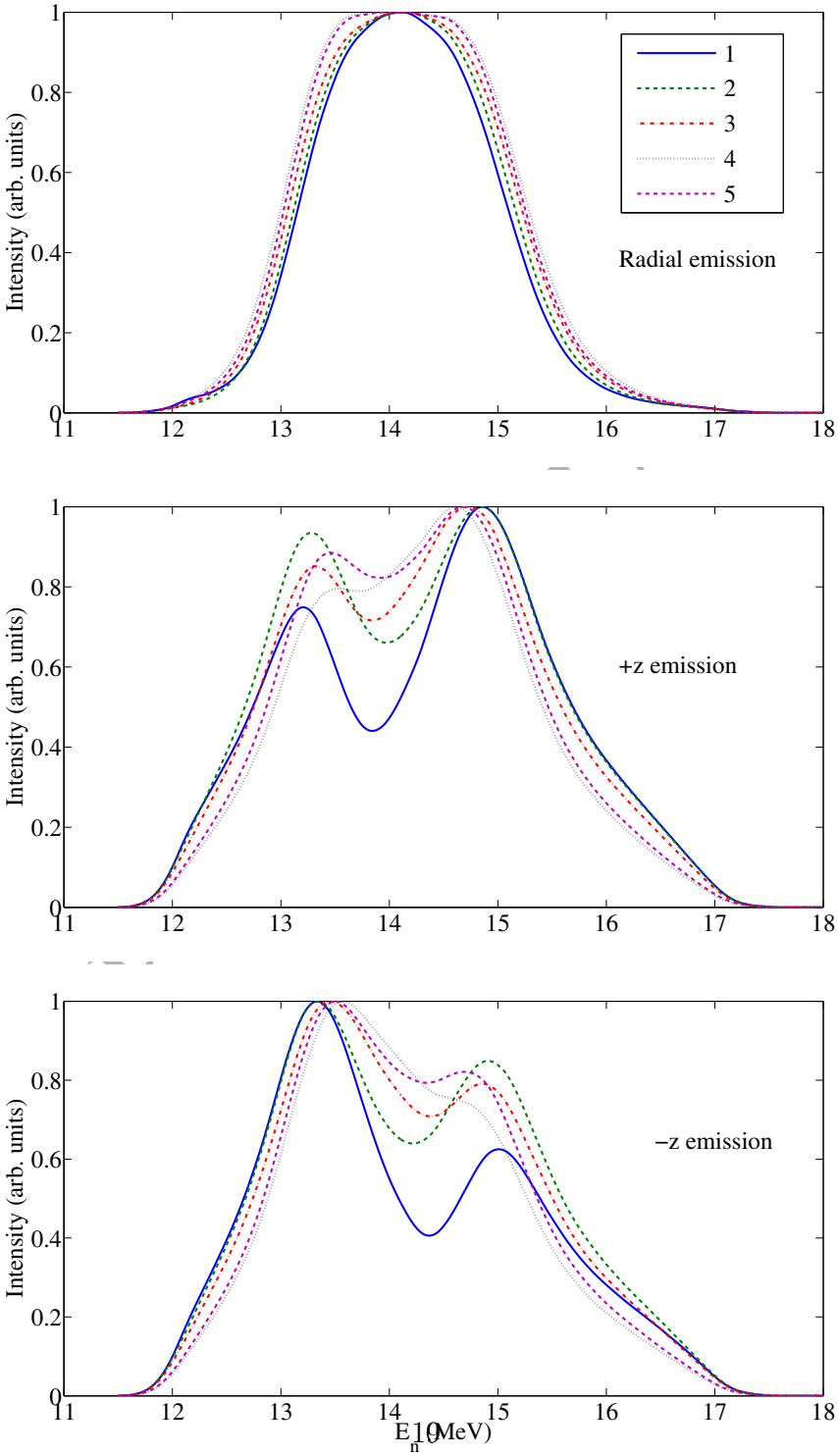

Figure 6: Secondary spectra results for simulations of the mirror topology. The parameters used to produce each set of spectra are listed in table 2. Spectra no. 1 is generated with $\langle BR \rangle = 0.3\,T\,m$ and a cylinder that is pinched at the bottom only. Pinching of the top end of the cylinder or further pinching of the bottom end of the cylinder both reduce the asymmetry of the axial spectra (as illustrated by spectra nos. 2 and 3, respectively). The asymmetry is also reduced for higher values of $\langle BR \rangle$. Spectra nos. 4 and 5 are both

5.1. Field parameterization for the helical topology

We assume that the central axis of the stagnated fuel follows a helical path of radius H_r and pitch H_p defined by

$$x = H_r \cos(t), \tag{14}$$
$$y = -H_r \sin(t), \tag{15}$$
$$z = \frac{H_p}{2\pi} t. \tag{16}$$

This describes a left-handed helix where t is the free parameter defining the curve. As t varies from 0 to 2π the helix completes one full revolution about the axis and undergoes an axial displacement of H_p. The helical tube of fuel has a radius R measured from this central axis. The **B** field at a given height z is in the direction tangential to the central axis at that height. We assume that the strength of the field is uniform throughout the helical tube and is defined by the $\langle BR \rangle$ parameter. Therefore, the **B** field within the helical tube is a function of z as follows

$$B_x = -\frac{\langle BR \rangle}{R} \frac{H_r}{\sqrt{H_r^2 + \left(\frac{H_p}{2\pi}\right)^2}} \sin\left(\frac{2\pi z}{H_p}\right), \tag{17}$$

$$B_y = \frac{\langle BR \rangle}{R} \frac{H_r}{\sqrt{H_r^2 + \left(\frac{H_p}{2\pi}\right)^2}} \cos\left(\frac{2\pi z}{H_p}\right), \tag{18}$$

$$B_z = \frac{\langle BR \rangle}{2\pi R} \frac{H_p}{\sqrt{H_r^2 + \left(\frac{H_p}{2\pi}\right)^2}}. \tag{19}$$

This **B** field topology will cause the tritons to undergo a drift motion due to the curvature of the field. For a left-handed helix with a B_z field component that points in the $+z$ direction this curvature drift will be in the $+z$ direction. If either the handedness or the **B** field direction is reversed then curvature drift will be in the $-z$ direction.

It is worth noting that the helical topology, like the azimuthal topology, causes an axial drift of tritons through the introduction of an azimuthal field component. However, singular orbits are not possible in the helical topology and so the triton dynamics are quite different in each case.

5.2. Secondary spectra for the helical topology

Figure 7 shows some of the most interesting results obtained for the helical topology. The corresponding parameter values are given in table 3. It is clear that the helical topology can produce axial spectra with significant asymmetry.

The spectra labelled 1 show a level of axial asymmetry such that the lower energy peak in the $+z$ direction has an intensity of approximately two-thirds that of the higher intensity peak, with the inverse in the $-z$ direction. This occurs for $\langle BR \rangle = 0.3\,T\,m$, $H_r = 100\,\mu m$ and $H_p = 1\,mm$. As H_r is reduced or H_p is increased (both causing the helical tube to become closer to a cylindrical column), the degree of asymmetry in the axial spectra is reduced. This is illustrated by spectra no. 2 and 3, respectively. For $\langle BR \rangle = 0.3\,T\,m$, the degree of asymmetry becomes negligible for $H_r <\sim 30\,\mu m$ or $H_p >\sim 2.5\,mm$.

As $\langle BR \rangle$ is increased above $0.3\,T\,m$ the axial spectra become more symmetric, as illustrated by spectra no. 4 and 5. Symmetry is recovered when $\langle BR \rangle$ reaches $\sim 0.6\,T\,m$.

It is also worth noting that the radial spectra in fig. 7 show an asymmetry near the spectral peaks. These peaks are also upshifted by $\sim 100\,keV$ to energies greater than $14.1\,MeV$. This is in contrast to the radial spectra for the azimuthal and mirror topologies which are more symmetric and with a peak energy close to $14.1\,MeV$. The asymmetry appears to be caused by the drift motion of the tritons in the helical topology. These tritons have a small drift component directed radially outwards, in addition to the axial drift. This causes radially emitted neutrons to have a mean energy slightly higher than the nominal value of $14.1\,MeV$. The radial asymmetry feature could potentially aid the diagnosis of the field conditions but further work is needed to study the sensitivity of this feature to changes in the field.

The yield ratios $\overline{Y}$ reported in table 3 are generally lower than those obtained for the other topologies and in experiment. This is because tritons born at a large radius have a greater chance of escaping when the fuel is in the shape of a helical tube rather than a cylinder. Therefore, increasing H_r and reducing H_p, which is necessary to produce asymmetry in the axial spectra, causes an increase in the fraction of tritons that are lost from the fuel early in time.

We can conclude from our study of the helical topology that significant asymmetry of the axial spectra can be produced using this topology for a

Table 3: This table lists data relating to the spectra plotted in fig. 7. The helical field topology parameters ($\langle BR\rangle$, H_r, H_p) used to generate each set of spectra are given together with the FWHM values of the spectra (Δ_R for the radial spectrum and Δ_{+z} for the axial spectrum). The ratio of secondary to primary neutron yields ($\overline{Y}$) for each simulation is also listed. The same values of T_{i0}, T_{iR}, ν, h, R and ρ_0 are used as in table 2. We note that the experimental images suggest a helix with a pitch of $1-2\,mm$ and radius of less than $100\,\mu m$.[8, 24]

Spec no.	$\langle BR\rangle$ $(T\,m)$	H_r (μm)	H_p (μm)	$\overline{Y}$	Δ_R (MeV)	Δ_{+z} (MeV)
1	0.3	100	1×10^3	4.22×10^{-3}	2.08	2.40
2	0.3	60	1×10^3	6.25×10^{-3}	1.83	2.71
3	0.3	100	2×10^3	7.68×10^{-3}	1.76	2.85
4	0.4	100	1×10^3	8.35×10^{-3}	1.99	2.46
5	0.5	100	1×10^3	1.44×10^{-2}	2.03	2.45

range of parameter values that are consistent with those inferred from the X-ray images of MagLIF experiments.

6. Secondary spectra produced from 1D MHD simulations

The above analysis has used steady-state profiles for the stagnated fuel conditions. We now use the Gorgon code[20] to carry out $1D$ MHD simulations which result in a time-varying stagnation phase. These simulations show that the current can penetrate through the liner resulting in an azimuthal **B** field in the fuel that affects the secondary spectra.

Figure 8 shows the results from one such simulation. The simulation has an initial fuel radius of $2.325\,mm$ and beryllium liner thickness of $465\,\mu m$. The initial fuel density is $0.7\,mg\,cm^{-3}$ and the fuel contains a seed axial **B** field of $5\,T$. The liner implosion is driven with a current which has a peak value of $18\,MA$. The fuel is artificially preheated to a temperature of $15\,eV$. This value was chosen as it produced stagnation phase results that best matched reported experimental results.[8] At $1\,ns$ intervals during the stagnation phase the fuel density, temperature, velocity and the **B** fields are outputted. This data is then post-processed using the same method as described in section 2. Triton particles are produced at regular intervals during the stagnation phase, weighted according to temperature and density, and transported using the time-varying MHD data.

The simulation results in a DD neutron yield of 10^{14} (for a pinch height

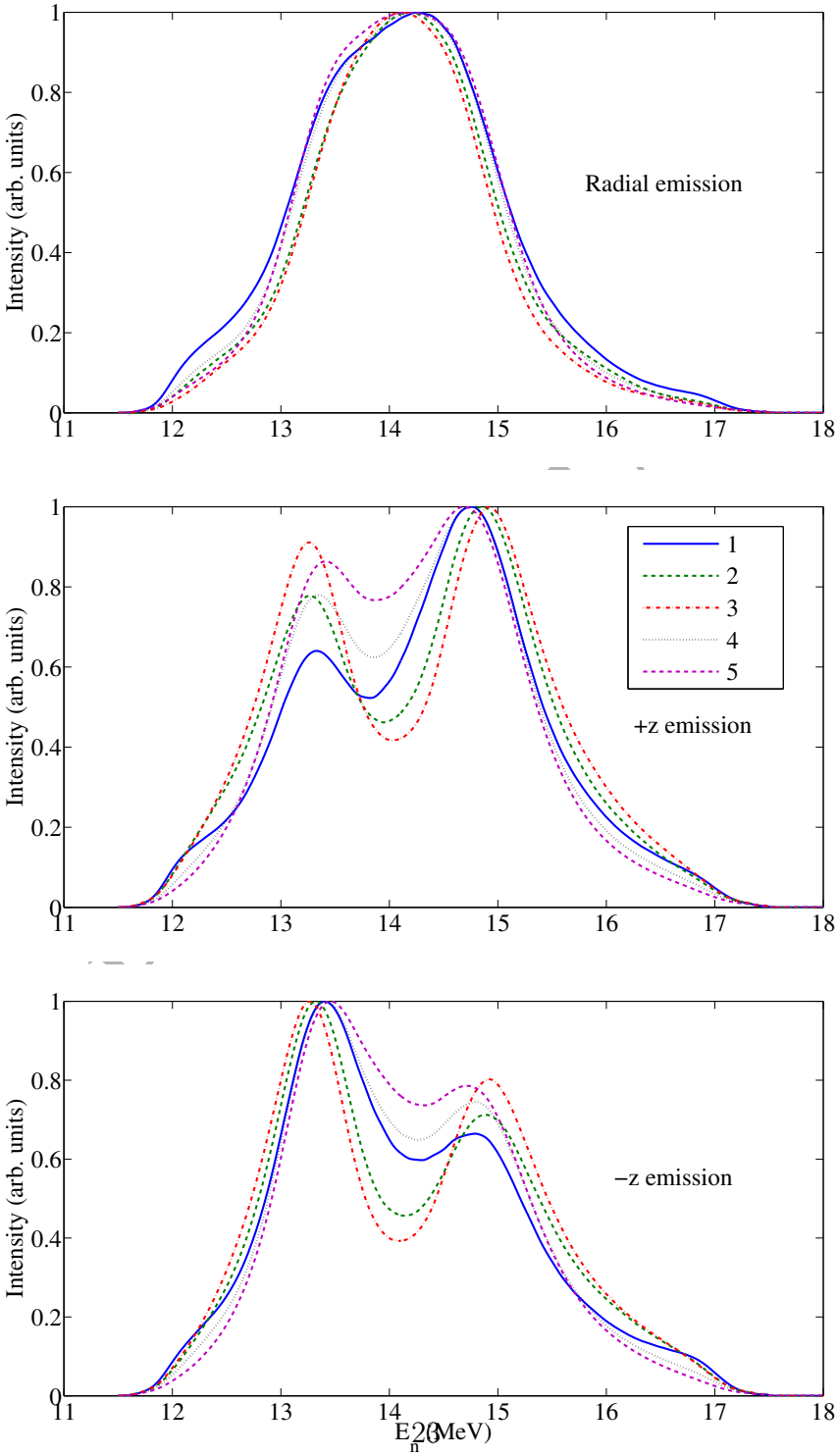

Figure 7: Secondary spectra results for simulations of the helical topology. The parameters used to produce each set of spectra are listed in table 3. Spectra no. 1, generated with $\langle BR \rangle = 0.3\,T\,m$, $H_r = 100\,\mu m$ and $H_p = 1 \times 10^3\,\mu m$, have a clear axial asymmetry. Reducing the helix radius or increasing the helix pitch both cause a reduction in the asymmetry. This is illustrated by spectra nos. 2 and 3 in which $H_r = 60\,\mu m$ and $H_p = 2 \times 10^3\,\mu m$, respectively. Increasing the value of $\langle BR \rangle$ also reduces the asymmetry, as

of $1\,cm$) and a secondary DT neutron yield of 1.9×10^{12}, giving a yield ratio of $\bar{Y} = 0.019$. The ion temperature inferred from the width of the time-integrated DD neutron spectrum is $2.23\,keV$. The top diagram of fig. 8 shows how the stagnation properties vary with time. During the $6\,ns$ burn pulse duration, the fuel reaches a peak ρR of $7.2\,mg\,cm^{-2}$, a peak $\langle BR \rangle$ of $0.4\,T\,m$ and a minimum radius of $45\,\mu m$. The lack of instabilities in the $1D$ simulation means that the burn pulse has a longer duration (resulting in a higher yield) than is expected in the experiment.

The bottom diagram of fig. 8 shows the time-integrated secondary DT spectra. There is a clear asymmetry of the axial spectra. This is due to diffusion of azimuthal $\mathbf{B}$ field from the liner into the fuel. At peak neutron output $\langle BR \rangle = 0.38\,T\,m$ and the azimuthal field profile corresponds approximately with that defined in section 3 with parameter values of $\gamma = 6$ and $\zeta = 0.27$.

As the initial fuel density used in simulations is increased from $0.7\,mg\,cm^{-3}$ to $1.5\,mg\,cm^{-3}$, it is found that the peak $\langle BR \rangle$ values and the secondary spectral shapes remain relatively constant. However, increasing the seed $\mathbf{B}$ field from $5\,T$ to $10\,T$ has a significant impact on the results. The peak $\langle BR \rangle$ value increases from $0.4\,T\,m$ to $0.6\,T\,m$ which causes the axially emitted secondary spectra to be almost symmetric. The increased seed field also causes a $\times 2.5$ increase in the value of $\bar{Y}$.

These $1D$ simulations give support to the hypothesis that azimuthal $\mathbf{B}$ field could be responsible for the shape of secondary spectra observed in experiments. MHD simulations of the mirror and helical topologies require suitably perturbed multi-dimensional simulations, which is beyond the scope of the present work.

7. Conclusions

We have demonstrated how the shape of secondary neutron spectra emitted from MagLIF experiments can be affected by both the strength and topology of $\mathbf{B}$ fields. Three classes of $\mathbf{B}$ field topologies were studied. Of these three classes, the azimuthal topology was the one which reproduced the asymmetry observed in experiment over the broadest range of parameters. Furthermore, the azimuthal topology was shown to be present in $1D$ MHD simulations. The helical topology also caused significant levels of asymmetry of the axial spectra in a parameter range relevant to experimental observations. In the case of the mirror topology, creating noticeable asymmetry of

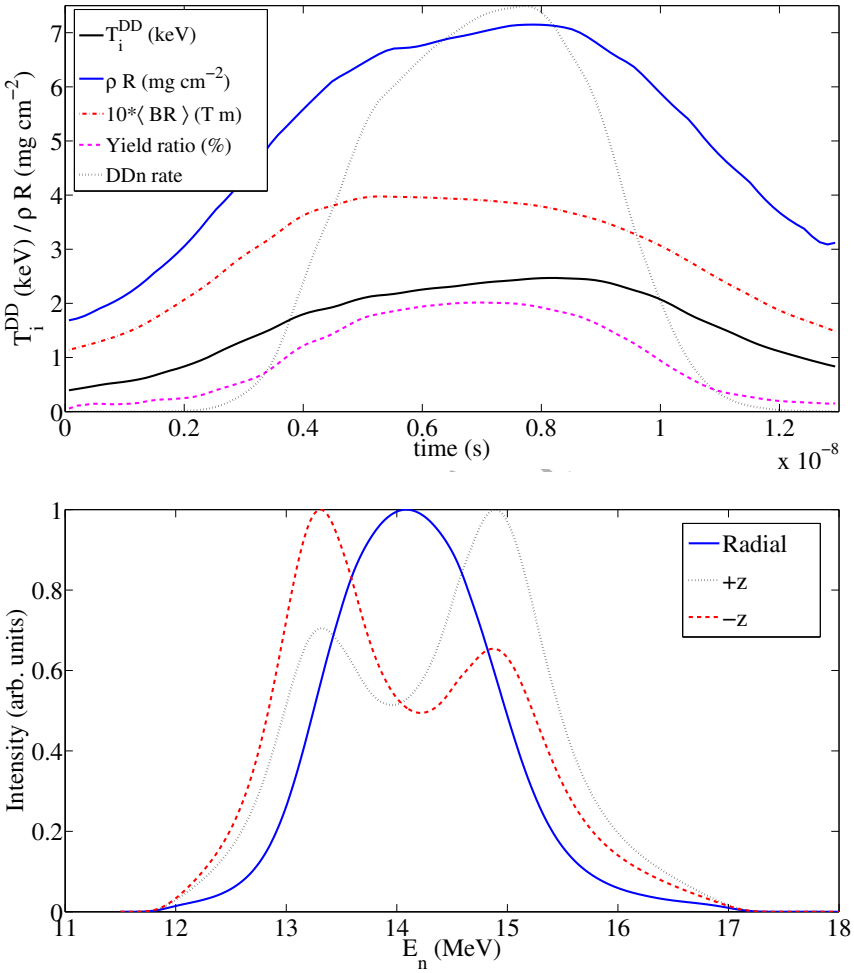

Figure 8: Top: Time evolution of the stagnation properties of a $1D$ Gorgon simulation. "DDn rate" denotes normalized rate of production of DD neutrons. T_i^{DD} denotes the ion temperature inferred from the width of the instantaneously produced DD neutron spectrum. Bottom: The time-integrated secondary neutron spectra produced from the simulation.

the axial spectra requires significantly different conditions to occur at one end of the fuel column compared with the other.

The purpose of this work is not to conclusively identify the cause of the asymmetry in the axial spectra measured in MagLIF experiments. Instead, the aim is to motivate the use of secondary neutron spectra as a diagnostic of the **B** field topology by demonstrating how sensitive the secondary spectra are to changes in the field topology. Further work is required to reliably infer **B** field topology from secondary spectra in MagLIF experiments.

First, a greater amount of experimental data is required in order to understand how the spectral shapes relate to other experimental observables such as neutron yields and X-ray emission.

Secondly, further improvements to the model that we have used in this work are necessary to fully understand the link between **B** field topology and secondary spectral shapes. For example, preliminary tests have shown that varying the strength of the magnetic field with distance from the tube axis in the helical topology can cause changes to the spectral shapes compared with the uniform strength case that we have used here. Furthermore, we note that whilst varying the **B** field parameters causes a wide variation in the resulting values of $\overline{Y}$, Δ_R and Δ_{+z}, these values generally tend to be slightly lower than those recorded in experiment. Whether this can be corrected by varying the existing set of parameters or if other physical features (such as neutron scattering causing spectra to broaden) need to be modelled remains to be seen.

Finally, the effects of temporal and spatial inhomogeneities on the secondary spectral shapes needs to be investigated. For example, non-uniform production of tritons along the axis could affect the shape of axial spectra. Multi-dimensional simulations that model the growth of perturbations during implosions will be necessary to evaluate such effects.

Acknowledgements

The authors would like to thank Patrick Knapp and Paul Schmit for helpful discussions. The results reported in this paper were obtained using the UK National Supercomputing Service ARCHER and the Imperial College High Performance Computer Cx1. This work was supported by the Engineering and Physical Sciences Research Council through Grant Nos. EP/K028464/1 and EP/L000237/1 and by AWE Aldermaston.

References

[1] P. F. Schmit, et al., *Phys. Rev. Lett.* **113**, 155004 (2014).

[2] P. F. Knapp, et al., *Physics of Plasmas* **22**(5), (2015).

[3] M. Basko, A. Kemp, J. M. ter Vehn, *Nuclear Fusion* **40**(1), 59 (2000).

[4] I. Lindemuth, R. Kirkpatrick, *Nuclear Fusion* **23**(3), 263 (1983).

[5] S. A. Slutz, et al., *Physics of Plasmas (1994-present)* **17**(5), (2010).

[6] S. A. Slutz, R. A. Vesey, *Phys. Rev. Lett.* **108**, 025003 (2012).

[7] S. A. Slutz, et al., *Physics of Plasmas* **23**(2) (2016).

[8] M. R. Gomez, et al., *Phys. Rev. Lett.* **113**, 155003 (2014).

[9] M. D. Cable, S. P. Hatchett, *Journal of Applied Physics* **62**(6) (1987).

[10] H. Brysk, *Plasma Physics* **15**(7), 611 (1973).

[11] B. Appelbe, J. Chittenden, *High Energy Density Physics* **11**(0), 30 (2014).

[12] J. P. Chittenden, B. D. Appelbe, F. Manke, K. McGlinchey, N. P. L. Niasse, *Physics of Plasmas* **23**(5) (2016).

[13] B. Appelbe, J. Chittenden, *Plasma Physics and Controlled Fusion* **53**(4), 045002 (2011).

[14] C. Birdsall, A. Langdon, *Plasma Physics via Computer Simulation*, Series in Plasma Physics and Fluid Dynamics. Taylor & Francis (2004).

[15] L. Spitzer, *The Physics of Fully Ionized Gases*. Interscience Publishers (1956).

[16] M. Sherlock, *Journal of Computational Physics* **227**(4), 2286 (2008).

[17] B. Appelbe, J. Chittenden, *Physics of Plasmas (1994-present)* **19**(7), (2012).

[18] B. Appelbe, J. Chittenden, *Physics of Plasmas* **22**(10) (2015).

[19] M. B. Chadwick, et al., *Nuclear Data Sheets* **107**, 2931 (2006).

[20] J. D. Pecover, J. P. Chittenden, *Physics of Plasmas* **22**(10) (2015).

[21] M. G. Haines, *Nuclear Instruments and Methods in Physics Research* **207**(12), 179 (1983).

[22] M. G. Haines, *Journal of Physics D: Applied Physics* **11**(12), 1709 (1978).

[23] A. B. Sefkow, et al., *Physics of Plasmas* **21**(7), (2014).

[24] S. B. Hansen, et al., *Physics of Plasmas* **22**(5), (2015).

[25] T. J. Awe, et al., *Physics of Plasmas* **21**(5) (2014).